materials

MDPI

Review

Metal Oxide Compact Electron Transport Layer Modification for Efficient and Stable Perovskite Solar Cells

Md. Shahiduzzaman [1,*], Shoko Fukaya [2], Ersan Y. Muslih [3], Liangle Wang [2], Masahiro Nakano [3], Md. Akhtaruzzaman [4], Makoto Karakawa [1,2,3], Kohshin Takahashi [3], Jean-Michel Nunzi [1,5] and Tetsuya Taima [1,2,3,*]

1 Nanomaterials Research Institute, Kanazawa University, Kakuma, Kanazawa 920-1192, Japan; karakawa@staff.kanazawa-u.ac.jp (M.K.); nunzijm@queensu.ca (J.-M.N.)
2 Graduate School of Frontier Science Initiative, Kanazawa University, Kakuma, Kanazawa 920-1192, Japan; sheeepwing-tjkst@stu.kanazawa-u.ac.jp (S.F.); Bro.Wang@outlook.com (L.W.)
3 Graduate School of Natural Science and Technology, Kanazawa University, Kakuma, Kanazawa 920-1192, Japan; ersanmuslih@gmail.com (E.Y.M.); masahiro-nakano@se.kanazawa-u.ac.jp (M.N.); ktakaha@se.kanazawa-u.ac.jp (K.T.)
4 Solar Energy Research Institute, The National University of Malaysia, Bangi 43600, Malaysia; akhtar@ukm.edu.my
5 Department of Physics, Engineering Physics and Astronomy, Queens University, Kingston, ON K7L-3N6, Canada
* Correspondence: shahiduzzaman@se.kanazawa-u.ac.jp (M.S.); taima@se.kanazawa-u.ac.jp (T.T.); Tel.: +81-76-234-4937 (M.S.)

Received: 14 April 2020; Accepted: 9 May 2020; Published: 11 May 2020

Abstract: Perovskite solar cells (PSCs) have appeared as a promising design for next-generation thin-film photovoltaics because of their cost-efficient fabrication processes and excellent optoelectronic properties. However, PSCs containing a metal oxide compact layer (CL) suffer from poor long-term stability and performance. The quality of the underlying substrate strongly influences the growth of the perovskite layer. In turn, the perovskite film quality directly affects the efficiency and stability of the resultant PSCs. Thus, substrate modification with metal oxide CLs to produce highly efficient and stable PSCs has drawn attention. In this review, metal oxide-based electron transport layers (ETLs) used in PSCs and their systemic modification are reviewed. The roles of ETLs in the design and fabrication of efficient and stable PSCs are also discussed. This review will guide the further development of perovskite films with larger grains, higher crystallinity, and more homogeneous morphology, which correlate to higher stable PSC performance. The challenges and future research directions for PSCs containing compact ETLs are also described with the goal of improving their sustainability to reach new heights of clean energy production.

Keywords: metal oxide; compact layer; electron transport layer; modification layer; perovskite solar cells

1. Introduction

Energy is one of the fundamental necessities of our current society. At present, the ever-increasing world energy consumption relies on fossil energy resources. Burning fossil fuels releases greenhouse gases, causing global warming, which threatens the Earth's ecosystems. Therefore, it is strongly desired to explore alternative, carbon-free, renewable energy sources to replace fossil fuels. Solar energy is an attractive alternative energy source because it is the largest usable source that could potentially meet global future energy demands. A solar cell is a device that converts solar energy directly into electrical

energy. Solar cells make no noise or pollution and have no moving parts, making them robust, reliable, and long-lasting [1–3]. The development of alternative power systems that harvest ambient energy sources (radiant, thermal, and mechanical energy) is desired in order to perpetually power or recharge Internet of Things devices. Solar cells possess several advantageous features, including high stability and a cost-effective fabrication process. Because of these features, solar cells are expected to act as long-term power supplies for satellites and space vehicles [4].

The majority of research on solar cells has focused on silicon-based assemblies, in which silicon is used as both the light absorber and charge transporter [5]. However, the high processing cost, toxicity of silicon-based chemicals, and high energy demands for cell fabrication are disadvantages that currently limit the wide application of silicon-based solar cells. The buildings where such solar cells can be installed are limited. Researchers have been exploring potential next-generation solar cell technologies that are cheap and can be processed using simple solution-based techniques. Solution-based processing has been used to fabricate various types of photovoltaic cells, such as organic photovoltaics, dye-sensitized solar cells, quantum dot solar cells, and perovskite solar cells (PSCs), making these cells attractive lost-cost alternatives to silicon solar cells.

Perovskites are minerals with the same structure as calcium titanium oxide ($CaTiO_3$) and are named after the Russian Geographical Society founder Lev Perovski. The light harvester in PSCs is a perovskite such as methylammonium lead iodide ($CH_3NH_3PbI_3$), with a general formula ABX_3, where "A" is a univalent organic cation ($CH_3NH_3^+$), "B" is a bivalent metal ion (Pb^{2+}) and "X" is a halide (I^-) anion (Figure 1a). Here, A coordinates with 12 X anions and B coordinates with six X anions, forming a geometry of cubes and octahedrons, respectively. The crystal structure and perovskite arrangement can be estimated using the Goldschmidt tolerance factor. Hybrid organic–inorganic metal halide PSCs are currently the fastest growing technology in the history of photovoltaics. Such PSCs have attracted broad interest from academic and industrial communities because of their favorable optoelectronic properties, such as tunable bandgap, high absorption coefficient, high electron and hole mobilities, long diffusion lengths (>1 μm), and easy and inexpensive fabrication by solution processing [6–9]. Intensive research efforts around the world have led to great improvements in the power conversion efficiency (PCE) of PSCs since their original PCE of 3.8% was reported by Miyasaka and co-workers in 2009 [10]. In just over a decade, the PCE of PSCs has rapidly increased to reach the latest record of 25.2%, approaching the top values achieved for single-crystalline silicon solar cells [11]. There are two leading types of device architecture that yield efficient PSCs: planar heterojunctions (PHJs) and mesoporous (mp) structures. Because of their facile device processing and efficient performance, PHJ PSCs have attracted more research interest than mp-PSCs. Typical PSCs have a sandwich structure consisting of a perovskite photoactive layer with a thickness of several hundred nanometers between metal oxide (MO_x) layers; namely, an electron transport layer (ETL) and hole-transport layer (HTL) (Figure 1b). When a perovskite device is illuminated by a standard simulated solar spectrum, charge carriers are generated within the perovskite photosensitive layer, separated by the ETL and HTL, and collected at their respective electrodes, thereby generating an electric current. A schematic illustration of the energy-level alignment between device components is shown in Figure 1c. The ETL needs to transport photogenerated electrons and block holes to eradicate the electrical shunt and afford stable PSCs with high performance. Figure 1d shows the progress in PSC efficiency by year.

With the rapid improvement of PSC performance, device lifetime (operational stability) has become the main concern for their future commercialization. PSC stability can be affected by both extrinsic (environmental) and intrinsic factors. Environmental factors include moisture, oxygen, light, and heat, which can degrade the photoactivity of the perovskite components [12]. The intrinsic stability of perovskites is strongly influenced by the presence of defects in the perovskite layer and at the interface between the perovskite and charge transport layers [13]. Perovskite instability is dominated by the hygroscopic nature of the organic cations, under-coordinated lead atoms, thermal instability, and ion migration. The PSC degradation driven by the hygroscopic character of the organic cations is correlated with environmental factors, which can be resolved by device encapsulation [14]. Thermal

instability can be addressed by compositional engineering of the perovskite and inorganic materials used in the HTL [15–17]. Recently, Miyasaka et al. reported the design and fabrication of high-quality perovskite films and dopant-free HTLs for efficient and stable PSCs [18]. Ion migration in perovskite films is another origin of PSC degradation. Ion migration initiated by the illumination-induced electric field can be hindered or even stopped by passivating the grain boundaries in the device; that is, through interfacial modification [19]. Furthermore, ion substitution can decrease the packing density of the crystal lattice [20]. Interfacial modification can also lower the density of recombination hubs correlated with under-coordinated lead atoms or organohalide defect sites, consequently improving the overall PSC performance [21]. Modification of the ETL/perovskite interface plays roles in facilitating charge transport and suppressing hysteresis and interfacial recombination to realize highly efficient and stable PSCs [22]. Therefore, it is immensely desirable to develop facile techniques for the modification of ETL/perovskite interfaces to enable efficient fabrication of low-cost and highly stable PSCs. The present mini-review summarizes recent progress on MO_x compact ETLs and their systemic modification to realize high-efficiency and stable PSCs.

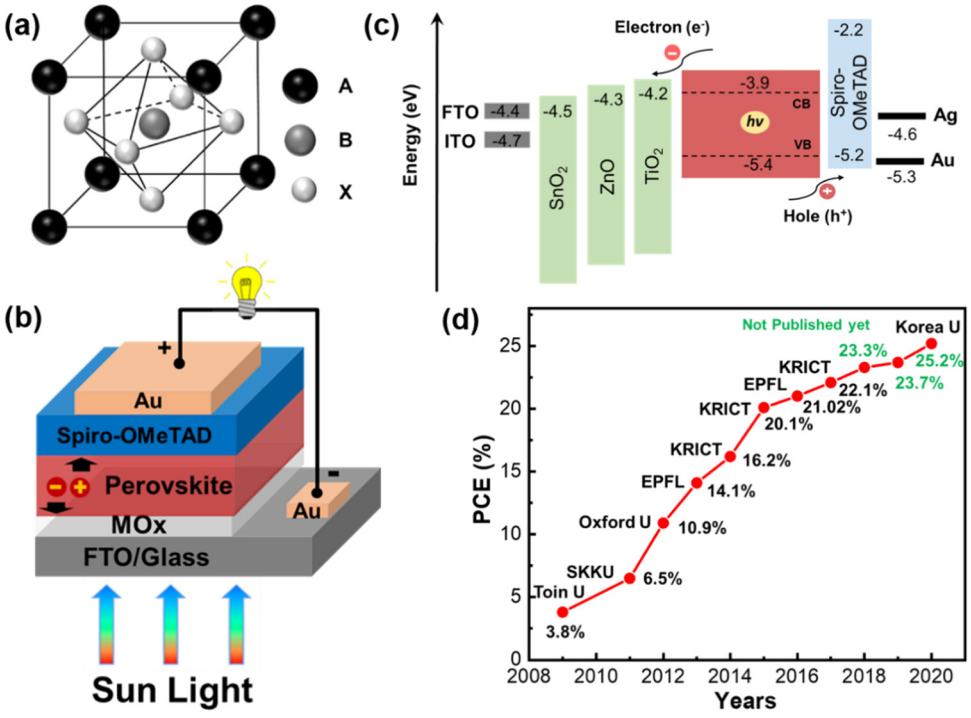

Figure 1. (**a**) General structure of a perovskite, (**b**) schematic of a perovskite solar cell with various layers, (**c**) energy band alignment of $MAPbI_3$ perovskite and various metal oxide electron transport materials in the device, and (**d**) performances evolution of perovskite solar cells certified by National Renewable Energy Laboratory (NREL) (14.1% [23], 16.2% [24], 20.1% [25], 21.02% [26] and 22.1% [27]). The green power conversion efficiencies (PCEs, 23.3%, 23.7%, and 25.2%) are not in the public domain yet. SKKU, EPFL, and KRICT denote Sungkyunkwan University, École polytechnique fédérale de Lausanne, and Korea Research Institute of Chemical Technology, respectively.

2. Metal Oxide Compact Electron Transport Layers

MO_x is the most uplifting design with respect to the thin-film processing, electronic structure, charge transport mechanisms, defect states, and optoelectronic properties [28]. However, MO_x are promising materials in PSCs because they suppress the electrical shunt between the transparent electrode/perovskite and transparent electrode/HTL interfaces as well as permitting electron transport and blocking hole transport to the respective electrode [29,30]. MO_x compact electron transport materials such as titanium dioxide (TiO_2) [31], zinc oxide (ZnO) [32], tin oxide (SnO_2) [33], zinc stannate

(Zn_2SnO_4) [34], zirconium dioxide (ZrO_2) [35], tungsten oxide (WO_3) [36], and niobium pentoxide (Nb_2O_5) [37], can be used as compact ETLs. In particular, efficient PSCs have been fabricated using TiO_2, SnO_2 and ZnO films as ETLs.

3. Titanium Dioxide (TiO_2)

The anatase (tetragonal), brookite (orthorhombic), and rutile (tetragonal) polymorphs of TiO_2 possess distinct crystalline phases and unique properties and have been widely used as photocatalysts [38] and in solar cells [39]. TiO_2 is the most promising material used in n-type ETLs for efficient PSCs because of its environmentally friendly nature, tunable electronic properties, low cost, and conduction band that is well matched with that of perovskites, thus facilitating electron injection and collection. However, the use of TiO_2 film in PHJ PSCs has the following drawbacks. (i) The low conductivity and electron mobility of TiO_2 are unfavorable for electron collection and transport [40,41]. (ii) Exposure of TiO_2 to ultraviolet light induces the formation of oxygen vacancies at the surface and grain boundaries of TiO_2 that act as charge traps and result in severe loss of photogenerated carriers through recombination [42,43]. Thus, the interface between TiO_2 and perovskite retards the photoresponse of the resultant devices and leads to strong hysteresis [41]. Considerable effort has been devoted to improving the performance of PSCs by resolving these drawbacks by modification of TiO_2 compact layers (CLs) via interface engineering and elemental doping. The surface morphology and properties of the TiO_2 CL of PSCs strongly affect the quality of the perovskite photosensitive layer in terms of the crystal size, homogeneity, and surface coverage, which in turn influence the photovoltaic performance [44]. The systemic modification of TiO_2 ETLs is important to optimize the efficiency and stability of PSCs.

3.1. TiO_2 Compact Layers (CLs)

PHJ PSCs with TiO_2 ETLs have received more research interest than mp-architectures because of their potential to realize low-temperature processing, simple device framework, and high-throughput roll-to-roll manufacturing. Optimization of deposition methods of TiO_2 CLs is important to achieve uniform compact thickness to maximize the charge transport capacity between the TiO_2 CL and perovskite. In addition, the thickness of the TiO_2 CL needs to be optimized to maximize electron transport from the perovskite to the fluoride-doped tin oxide (FTO) electrode. When the TiO_2 CL is too thick, the resultant increase of the distance of electron transport from the perovskite to FTO lowers the efficiency of charge transport [45]. Conversely, a TiO_2 CL that is too thin cannot efficiently cover the FTO substrate. Numerous deposition techniques have been used to form TiO_2 CLs in PSCs, such as the sol–gel method [46], oblique electrostatic inkjet (OEI) deposition, chemical bath deposition (CBD) [47,48], spray pyrolysis [49], atomic layer deposition (ALD) [50], thermal oxidation [31], sputtering [51], chemical vapor deposition (CVD) [52], and electrodeposition [53]. Spin coating is a commonly used simple and robust technique to form TiO_2 CLs. However, this approach cannot produce high-quality TiO_2 CLs and has limited suitability for large-scale production. Spray pyrolysis sprays a titanium precursor onto a heated substrate using an atomizer. The precursor droplets thermally decompose to form a TiO_2 CL. The TiO_2 CLs produced through either spin coating or spray deposition are particularly sensitive to control parameters. Consequently, the PCE of PSCs may differ considerably even when using the same technique to form TiO_2 CLs. ALD is a scalable technique for the preparation of TiO_2 CLs, but is relatively time consuming and expensive. CVD and sputtering require vacuum conditions and have slow deposition rates, which make them expensive and inconvenient for the production of TiO_2 CLs. Below, we discuss a few commonly used simple and efficient approaches to pattern TiO_2 CLs for PSCs.

3.1.1. Sol–Gel Technique

The sol–gel approach is widely considered to be a promising technique for the deposition of TiO_2 CLs because of its simplicity. Segawa and co-workers demonstrated the surface treatment of

TiO_2 CLs using an aqueous solution of $TiCl_4$ and ultraviolet/ozone to enhance the wettability and interface adhesion between the TiO_2 CL and perovskite [54]. The resultant PHJ PSCs showed PCEs of up to 16.9%. Zhou et al. reported planar PSCs with a PCE of 19.3% based on indium tin oxide (ITO)-coated glass treated with ethoxylated polyethyleneimine and a low-temperature TiO_2 CL [55]. In addition, to increase the conductivity of the TiO_2 CL, it was doped with yttrium. The favorable band alignment of yttrium-doped TiO_2 with the perovskite and ITO facilitated efficient electron injection and collection and suppressed interfacial recombination. Choi et al. reported PHJ PSCs with a PCE of 16.3% containing TiO_x CLs formed by a simple sol–gel process at room temperature [56]. The performance of these PSCs was comparable to that of cells containing TiO_2 CLs fabricated at high temperature. Additionally, the room temperature-processed TiO_x CL was used as an ETL in a flexible PSC that achieved a PCE of 14.3%. Liu et al. treated low-temperature-processed TiO_2 CLs with various concentrations of aqueous $TiCl_4$ solutions to form ETLs that were uniform, pinhole-free, and had full surface coverage [57]. PSCs containing these ETLs showed efficient electron transport, charge extraction, and suppressed charge recombination, which led to enhanced photovoltaic performance.

3.1.2. Chemical Bath Deposition (CBD)

CBD is a simple, inexpensive, convenient, and scalable technique to pattern TiO_x CLs from aqueous solutions, making it advantageous for large-scale production of thin films for organic photovoltaic cells and PSCs [58]. Several reports have been published about CBD TiO_2-based PSCs. Recently, Liu and co-workers reported PSCs containing co-doped TiO_2 ETLs formed by low-temperature CBD with a PCE of 19.10% [59]. In addition, the group led by Takahashi and Kuwabara developed a technique to pattern TiO_x films at low temperatures and used them as ETLs in organic photovoltaic cells that exhibited a PCE of 3.8% under AM1.5G simulated sunlight [60]. TiO_2 CLs fabricated by CBD form good physical and electronic contacts with perovskite photosensitive layers. We reported PHJ PSCs with TiO_x CLs formed by CBD and modified with a thin layer of fullerene or a derivative as ETLs [47,48,61,62]. The scalable CBD technique solely enables production of TiO_x CLs at low temperature [63]. Photographs of the hydrolysis steps of CBD are shown in Figure 2. A 30 nm TiO_x film is formed in a single operation. The thickness of TiO_x can be increased by repeating the operation. However, it is quite difficult to control the morphology and thickness of TiO_2 CLs fabricated by CBD, which leads to poor reproducibility. Therefore, it remains important to develop a technique to fabricate high-quality TiO_2 CLs for efficient PHJ PSCs that is scalable, controllable, and low cost. This process can be used for roll-to-roll production, which may contribute it a potential candidate for low-cost commercial production of TiO_2-based ETLs in future solar modules.

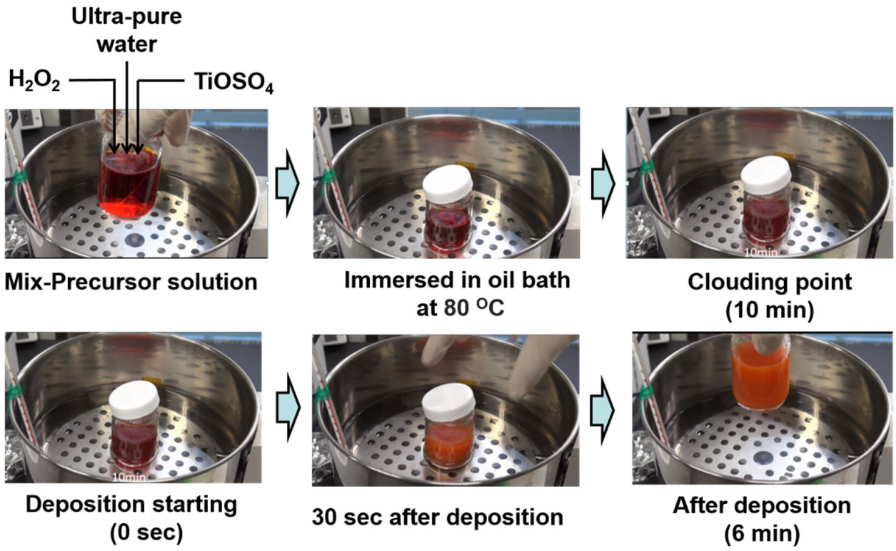

Figure 2. Photographs illustrating the hydrolysis steps in chemical bath deposition of TiO_x films.

3.1.3. Inkjet Printing Approaches

Inkjet printing is a scalable technique that is compatible with roll-to-roll processing. In addition, inkjet printing is cost-effective and has a high material utilization rate, which may lower the production cost of devices. Wei et al. reported efficient PSCs containing TiO_2 CLs formed by electrodeposition [53]. Electrodeposition is a simple, cost-effective, and scalable technique to pattern uniform TiO_2 CLs. The surface morphology and thickness of TiO_2 CLs can be controlled by simply manipulating deposition conditions. In addition, we recently developed an OEI bottom-up strategy to produce TiO_2 CLs that involves discharging a spray using electrostatic force. In the OEI strategy, an FTO substrate was patterned with a TiO_2 precursor solution using an ejection angle of 45° with respect to the substrate (Figure 3a). The OEI technique produced high-quality TiO_2 CLs on FTO substrates, which were used as the ETL in PSCs that showed a PCE of 13.19% [64]. Unlike other bottom-up techniques, OEI deposition offers a simple and cost-effective way to obtain high-quality TiO_2 films with easy-to-control thickness. Using OEI deposition, large-area stacked thin films can be fabricated with high reproducibility. The surface morphology of TiO_2 films was tuned by simply changing the coating time. Large-scale printing using OEI deposition may be realized by changing the single nozzle system to one with multiple nozzles. OEI deposition can be used to pattern a variety of substrates on a large scale to achieve high-throughput, large-area perovskite solar modules. The scalability, large-area uniformity, and low-cost fabrication capability with a high material utilization rate of OEI deposition might lower the production cost of resultant devices. This simple technique to fabricate TiO_2 CLs may help to further improve the photovoltaic performance of planar small- and large-scale PSC modules.

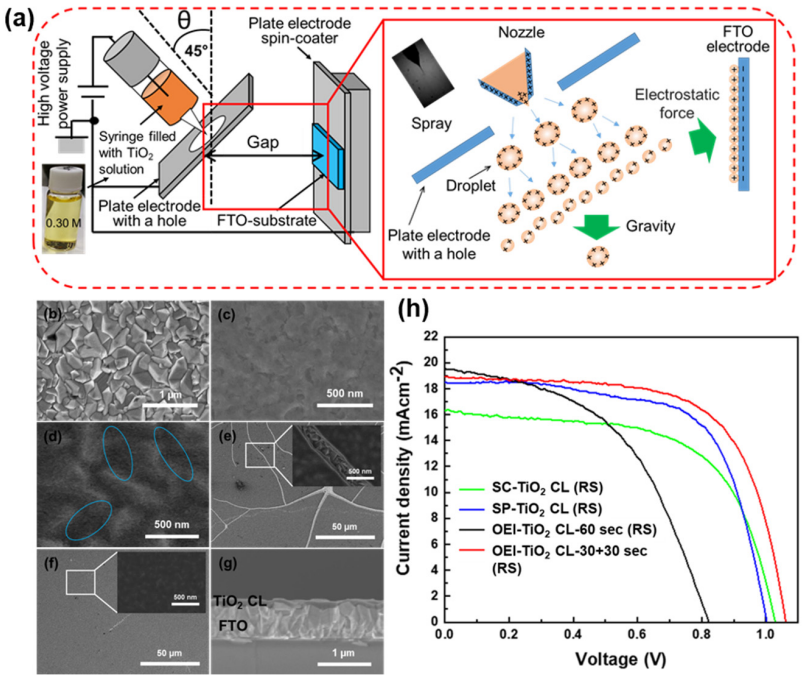

Figure 3. (**a**) Schematic of the oblique electrostatic inkjet (OEI) setup used to pattern TiO_2 compact layers (CLs) on fluoride-doped tin oxide (FTO)-coated glass substrates. Top-view scanning electron microscope (SEM) images of (**b**) bare FTO, (**c**) spin coating (SC)-TiO_2 CL, (**d**) spray pyrolysis (SP)-TiO_2 CL, (**e**) OEI-TiO_2 CL-60 s, and (**f**) OEI-TiO_2 CL-30 + 30 s. (**g**) Cross-sectional SEM image of the OEI-TiO_2 CL-30 + 30 s film. (**h**) Reverse *J-V* characteristics of perovskite solar cells (PSCs) made under different conditions. Reproduced with permission [64]. Copyright 2019, Springer Nature.

3.2. *Surface Modification by TiO_2 Nanoparticles*

To improve the performance and stability of PSCs, there has been significant focus upon the surface modification of ETLs. TiO_2 nanoparticles (NPs) possess a higher specific surface area than that

of TiO_2 CLs, enabling the surface morphology of TiO_2 films to be tuned. TiO_2 NPs can promote efficient electron injection and transport to improve the balance of charge carriers. The anatase phase of TiO_2 is extensively used as the ETL in PSCs because of its easy synthesis. Conversely, the brookite phase of TiO_2 is the least explored because it is difficult to synthesize the pure brookite phase. The rutile phase of TiO_2 also shows potential for use as an ETL in PSC applications. TiO_2 CLs composed of mixtures of anatase and rutile phases have been used in PSCs. To explore the performance of different polymorphs of TiO_2-based PSCs, it is important to understand the effect of TiO_2 microstructure on PSC performance and stability. At present, inorganic metal oxides (TiO_2 NPs, mp-TiO_2) and organics such as self-assembling monolayers (SAM), fullerene (C_{60}), [6,6]–phenyl–C_{61}–butyric acid methyl ester (PCBM) based materials are used to combine with or modify TiO_2 CL, SnO_2, ZnO in PSCs and their corresponding device architectures and PCEs are included in Table 1.

Table 1. Examples of surface modification of TiO_2, SnO_2 and ZnO CL in PSCs. The corresponding device architectures and PCEs are derived.

Surface Modification	Devices Structure	PCE (%)	Ref.
TiO_2/anatase TiO_2 NPs	FTO/TiO_2/anatase TiO_2 NPs/$MAPbI_3$/Spiro/Au	17.1	[65]
TiO_2/brookite TiO_2 NPs	FTO/TiO_2/brookite TiO_2NPs/$Cs_{0.05}(FA_{0.83}MA_{0.17})_{0.95}Pb(I_{0.83}Br_{0.17})_3$/Spiro/Au	16.8	[66]
TiO_2/brookite TiO_2 NPs	FTO/TiO_2/brookite TiO_2NPs/$MAPbI_3$/Spiro/Au	18.2	[67]
TiO_2/mp-TiO_2	FTO/TiO_2/mp-TiO_2/$Cs_{0.05}(FA_{0.83}MA_{0.17})_{0.95}Pb(I_{0.83}Br_{0.17})_3$/Spiro/Au	21.1	[44]
TiO_2/rutile TiO_2 NRs	FTO/TiO_2/rutile TiO_2 NPs/$MAPbI_3$/Spiro/Ag	18.2	[68]
TiO_2/C60	ITO/TiO_2/C60/$MAPbI_3$/Spiro/Ag	9.5	[47]
TiO_2/PDI-glass	ITO/TiO_2/PDI-glass/$MAPbI_3$/Spiro/Au	5.7	[61]
TiO_2/PNP	ITO/TiO_2/PNP/$MAPbI_3$/Spiro/Ag	8.2	[48]
TiO_2/SnO_2	FTO/TiO_2/SnO_2/$MAPbI_3$/PATT/Au	19.8	[69]
TiO_2/SnO_2	FTO/TiO_2/SnO_2/$FA_{0.83}MA_{0.17}(Ge_{0.03}Pb_{0.97}(I_{0.9}Br_{0.1})_3$/Spiro/Au	22.1	[70]
TiO_2/SnO_2	FTO/TiO_2/SnO_2/$MAPbI_3$/Spiro/Ag	21.1	[71]
TiO_2/SnO_2	ITO/TiO_2/SnO_2/$FA_{0.95}Cs_{0.05}PbI_3$/PCBM/Ag	21.5	[72]
SnO_2/SAM	FTO/SnO_2/SAM/$MAPbI_3$/Spiro/Au	18.8	[73]
SnO_2/PCBM	FTO/SnO_2/PCBM/$MAPbI_3$/Spiro/Au	19.1	[74]
ZnO/SnO_2	FTO/SnO_2/PCBM/$MAPbI_3$/Spiro/Ag	12.17	[75]
ZnO/SAM	ITO/ZnO/SAM/$MAPbI_3$/Spiro	13.7	[32]

3.2.1. Anatase TiO_2 Nanoparticles (NPs)

We found that introduction of single-crystalline anatase TiO_2 NPs, which were synthesized by a hydrothermal approach [76], between the TiO_2 CL and perovskite layer altered the interface surface morphology to provide highly efficient and stable PSCs [65]. TiO_2 NPs are water soluble and have a low content of carbon per titanium atom, which make them attractive reagents to prepare titanium-containing functional materials. Large grains with fewer grain boundaries were observed in the perovskite layer when TiO_2 NPs were introduced between the TiO_2 CL and perovskite, which facilitated efficient electron extraction and suppressed charge carrier recombination. PSCs containing the TiO_2 CL/anatase TiO_2 NP bilayer showed a PCE of 17.05% and decreased hysteresis (Figure 4) compared with that of the equivalent device without TiO_2 NPs. We also investigated the moisture stability of these bilayer-based PSCs stored a dry, dark N_2 environment. The PCE of the bilayer-based device showed remarkable long-term moisture stability, deteriorating to 38% of its initial PCE after 47 days. Gan et al. fabricated PSCs with a PCE of up to 3.7% by using TiO_2 nanorods with a length of 600 nm as an ETL scaffold [77]. He and his colleagues reported efficient PSCs containing an ETL of single-crystalline TiO_2 nanorods with an average length of 30 ± 10 nm and diameter of 4 ± 1 nm that exhibited a PCE of over 17% [78]. The one-dimensional nanostructure acted solely as a CL in the high-performance PSCs. In other work, high-performance stable PSCs were produced by adding TiO_2 NPs to a perovskite precursor solution to tune the perovskite morphology [79]. The tuned perovskite morphology improved electron extraction, thereby enhancing the PCE of the PSCs to 19.2%.

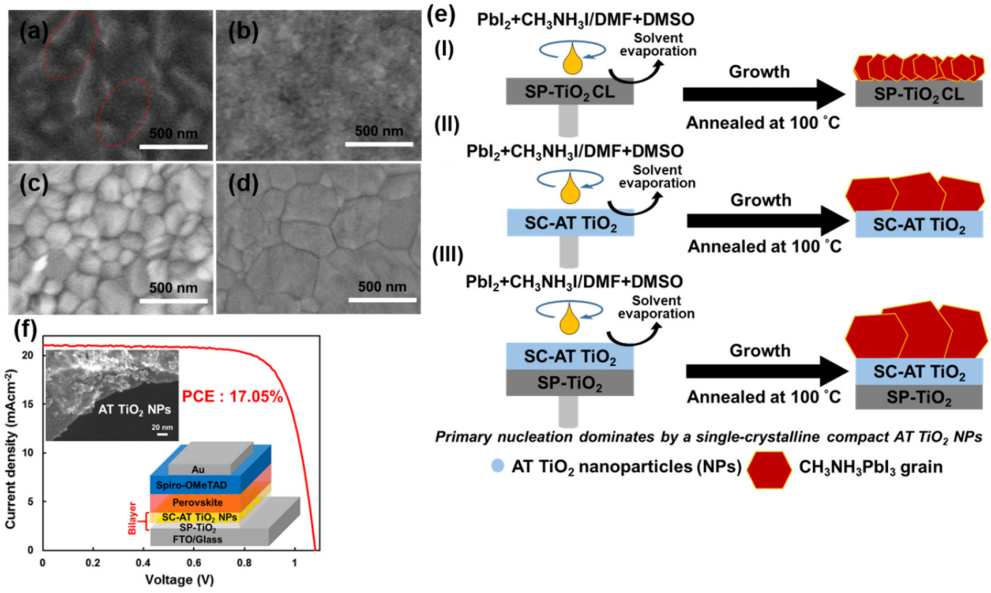

Figure 4. SEM images of the (**a**) SP-TiO_2 layer and (**b**) SP-TiO_2/SC-anatase (AT) TiO_2 nanoparticle (NP) bilayer and perovskite films grown on the (**c**) SP-TiO_2 layer and (**d**) SP-TiO_2/SC-AT TiO_2 NP bilayer. (**e**) Schematic of the nucleation and growth of perovskite grains. (**f**) Reverse *J-V* curve obtained for a solar cell with the NP bilayer. Insets shows the device structure and an SEM image of the NPs. Reproduced with permission [65]. Copyright 2018 American Chemical Society.

3.2.2. Brookite TiO_2 NPs

Among the three polymorphs of TiO_2, the brookite phase has been used the least in PSCs because it is difficult to synthesize. However, using brookite TiO_2 NPs instead of anatase TiO_2 in PSCs has numerous advantages. Compared with anatase TiO_2, brookite TiO_2 has (i) a higher driving force with more favorable energy-level alignment with the perovskite layer, (ii) higher capacity for charge transfer, (iii) increased crystallinity, (iv) synthesis at relatively low temperature, (v) higher conductivity, (vi) higher electron mobility to facilitate photogenerated electron collection, and (vii) higher thermal stability [80–82]. The conduction band edge of brookite is slightly higher than those of anatase and rutile TiO_2, which is expected to promote efficient electron transfer from the brookite to the anatase phase (Figure 5b). The close match of the conduction band edge of brookite with the band structure of perovskites might increase both the open-circuit voltage (V_{oc}) and efficiency of PSCs. The higher driving force with a more negative flat-band potential and more efficient charge separation and lower resistance of the brookite phase of TiO_2 with perovskite can be compared with the case for the anatase phase [80]. Charge transport at the semiconductor/electrolyte interface can be influenced by the semiconducting properties of the TiO_2 phase because the brookite phase shows higher conductivity and thermal stability than the anatase [81]. Miyasaka and co-workers fabricated compact TiO_x/mp-brookite TiO_2-based PSCs with a PCE of 21.6% and high V_{oc} because of the relative conduction-band level of the brookite layer to that of the perovskite [83]. PSCs with brookite TiO_2 exhibited a higher V_{oc} than those with other phases of TiO_2. Thus, it is important to explore the performance of PSCs containing ETLs composed of single-phase anatase or brookite and those with anatase-brookite (AB) and brookite-anatase (BA) heterophase junctions to best manipulate the charge transport characteristics of each phase. Recently, we fabricated TiO_2 heterophase junctions at low temperature (<180 °C) and tested their performance in PSCs. We used different TiO_2 phases to manipulate the charge transfer in TiO_2 semiconductor junctions in PSCs (Figure 5d,f). We also found that PSC efficiency can be improved by changing the crystalline phase of the TiO_2 CL. We showed that PSCs with FTO-AB as an ETL exhibited high efficiency up to 16.82% [66]. In addition, the results suggested that single-phase brookite TiO_2 NPs without a TiO_2 CL can act as an effective ETL in PSCs. These PSCs exhibited a

PCE of 14.92%, which was comparable to the first work reported by Miyasaka and co-workers [83]. Because of their suitable internecking particles to particles structure, single-phase brookite TiO_2 NPs can block holes effectively. The large specific surface area of brookite TiO_2 NPs allows efficient electron injection and subsequent transport that can balance the electron and hole current densities, strongly influencing the performance of PSCs. The rod-like brookite TiO_2 particles used in these PSCs ranged from 30–50 nm in diameter (Figure 5a). Such particles form a porous scaffold film rather than a CL. These particles cannot be considered as mp-materials because they do not contain pores. According to International Union of Pure and Applied Chemistry (IUPAC) nomenclature, mp-materials possess pores with diameters of 2–50 nm. The performance and stability of PSCs are strongly influenced by the nature of the underlying substrate. Recently, we reported that the incorporation of brookite TiO_2 NPs as a bridge between the TiO_2 CL and perovskite layer resulted in PSCs with highly reproducible PCEs of up to ~18.2% with stable performance of 18% under continuous one-sun illumination during maximum power point tracking, light soaking, and ambient atmosphere (Figure 5g–i) [67]. In contrast, the corresponding planar device with only a TiO_2 CL exhibited a PCE of ~ 15%. Highly stable and conductive brookite TiO_2 NPs have been used as a bridge between perovskite and TiO_2 CLs [81]. The NPs facilitated efficient interfacial charge transfer and promoted large grain growth, consequently enhancing device stability and performance. These results indicate that brookite TiO_2 NPs can be considered an alternative to anatase TiO_2-based materials in efficient and stable PSCs.

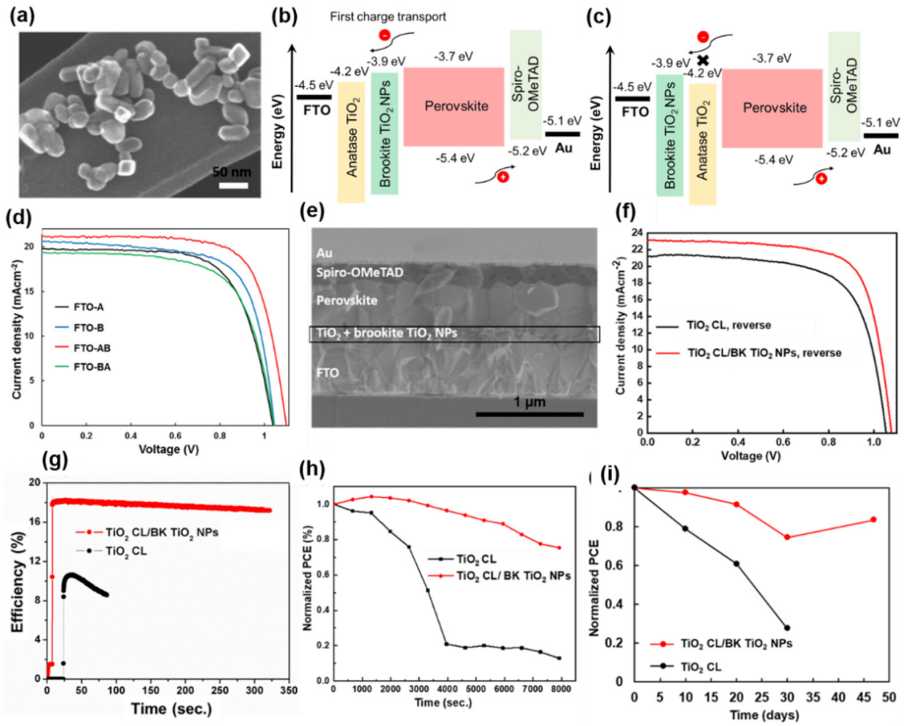

Figure 5. (**a**) Scanning transmission electron microscope (STEM) image of brookite (BK) TiO_2 NPs. Schematic illustrations of the energy-level alignment in devices with (**b**) FTO-anatase-brookite (AB) and (**c**) FTO-brookite-anatase (BA) as electron transport layers (ETLs). (**d**) *J-V* curves of PSCs with FTO-anatase (A), FTO-brookite (B), FTO-AB, and FTO-BA as ETLs. (**e**) Cross-sectional SEM image of the PSC with an FTO-AB ETL. (**f**) Reverse *J-V* curves obtained for the PSCs on substrates with and without a brookite (BK) TiO_2 NP layer. (**g**) Efficiency at maximum power point under continuous one-sun illumination (100 mW/cm^2). Reproduced with permission [66]. Copyright 2019 American Chemical Society. (**h**) Normalized PCE vs. time (in seconds) of TiO_2 CL/BK TiO_2 NP-based PSCs (non-encapsulated) after continuous exposure to one-sun illumination for 2.12 h in air with 60–70% relative humidity. (**i**) Normalized PCE versus time (in days) of PSCs (non-encapsulated) stored in the dark under dry N_2. The devices were measured under ambient conditions at 60–70% relative humidity. Reproduced with permission [67]. Copyright 2020, Royal Society of Chemistry.

3.2.3. Rutile TiO_2 NPs

The rutile TiO_2 phase also shows potential in PSC applications because it is easy to synthesize. Several studies on the application of highly crystalline, oriented rutile TiO_2 nanorods and nanowires in PSCs have been reported [84–87]. Park and co-workers reported efficient PSCs containing the rutile TiO_2 phase [88]. However, rutile TiO_2 has a more positive conduction band edge potential than that of anatase TiO_2, resulting in an inferior V_{oc} (Figure 6a). In addition, the inset shows more electrons injected to rutile TiO_2 which can lower the Fermi energy level at equilibrium between E_F (TiO_2) and E_F ($MAPbI_3$), resulting in the lower V_{oc} (Figure 6d). Subsequently, Wu et al. synthesized rutile TiO_2 NPs by CBD [89]. The NPs were introduced onto FTO substrates for use as the ETL in PSCs, which exhibited a PCE of 15.4% and high reproducibility. Li et al. reported a facile fabrication of TiO_2 nanorods by a solvothermal method [68]. The nanorods were incorporated in PSCs that exhibited a record PCE of 18.22%. These results demonstrated that the dense and uniform rutile TiO_2 NPs strongly suppressed hysteresis, which improved the long-term stability of the resultant PSCs. Shao and co-workers grew rutile TiO_2 thin films on FTO substrates by CBD [90]. PSCs containing these thin films exhibited PCEs of over 12%. This approach is an effective way to produce TiO_2-based PSCs at low temperature.

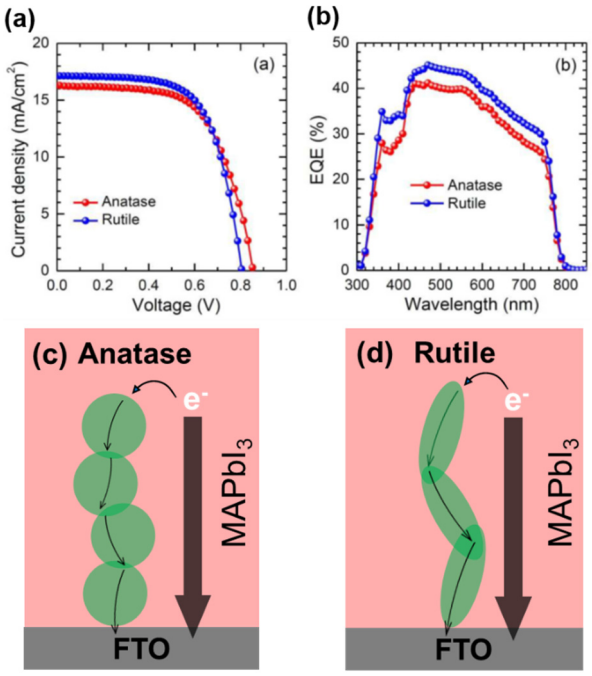

Figure 6. (**a**) *J-V* curves and (**b**) incident photon-to-current efficiency (IPCE) spectra of devices containing anatase and rutile TiO_2 thin films. Schematic of electronic behavior of devices with (**c**) anatase TiO_2 and (**d**) rutile TiO_2 films. Reproduced with permission [88]. Copyright 2014, Royal Society of Chemistry.

3.3. Mesoporous TiO_2

Generally, fabrication of mp-TiO_2 films requires a complicated and time-consuming process that involves deposition of a TiO_2 CL followed by synthesis of mp-TiO_2. In addition to altering the crystalline phase (anatase) of the amorphous oxide film, mp-TiO_2 requires a high-temperature sintering process at more than 500 °C to improve electron transport properties and remove polymer template molecules. Such a high-temperature, time-consuming process limits the application of mp-TiO_2 in flexible PSCs fabricated by roll-to-roll processing. Graetzel et al. studied the influence of lithium-doped mp-TiO_2 on the performance of PSCs [91]. These PSCs showed superior electronic properties because the lithium-doped mp-TiO_2 lowered electronic trap states, which enabled faster electron transport. Subsequently, Miyasaka and co-workers reported efficient PSCs with a PCE of 21.1% that showed

negligible hysteresis by introducing alkali-metal dopants into mp-TiO_2 (Figure 7) [44]. The doped TiO_2 films strongly modulated electronic conductivity, which improved charge extraction and hindered charge recombination. In addition, the doped TiO_2 thin film remarkably influenced the nucleation of the perovskite layer, which subsequently formed large grains that assembled into dense films with facetted crystallites. Huckaba et al. reported PSCs containing inkjet-printed mp-TiO_2 films that exhibited with a PCE of 18.29% [92]. Overall, inkjet printing technology provides a scalable and reliable alternative to spin coating for large-scale applications. Sung et al. developed PSCs containing mp-TiO_2 films composed of NPs with a size of 50 nm, which displayed promising performance, including a PCE of 17.19% [93]. Extensive effort has been expended developing nanostructure-based ETL materials for use in PSC applications. Wang et al. revealed that the introduction of a nanocomposite of graphene/TiO_2 NPs into mp-structured [94]. PSCs led to increased charge collection, which resulted in improved photovoltaic performance. Huang's group fabricated mp-TiO_2 nanopillars by room-temperature reactive magnetron sputtering [95]. The nanopillars were then used as the ETL in PSCs. The efficient TiO_2 CL/mp-TiO_2 nanopillar scaffold achieved fast carrier extraction and thereby suppressed recombination loss. Several other efficient mp-TiO_2-based PSCs have also been reported to date [96,97].

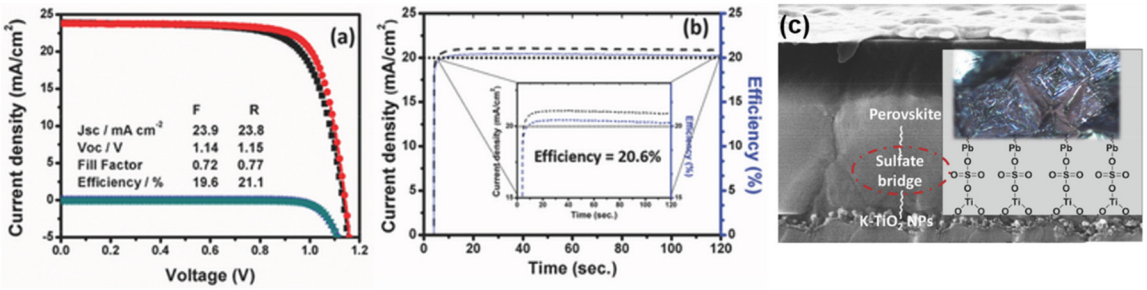

Figure 7. (**a**) *J-V* characteristics of the best-performing PSC fabricated on K2 substrates, which showed a PCE of 21.1% and V_{OC} of 1.15 V. (**b**) Steady-state PCE and J_{sc} at maximum power point of the best-performing device. Inset is a magnified image of the efficiency (blue dotted line) and Jsc (black dotted line)). (**c**) Combined cross-sectional SEM image and schematic of a doped TiO_2 mesoporous layer and the surface states bonding with the ETL and perovskite. Reproduced with permission [44]. Copyright 2018, Wiley-VCH Verlag GmbH & Co. KGaA, Weinheim.

3.4. Tin Dioxide

SnO_2 can be considered other potential ETLs widely used in PSCs owing to their favorable optoelectronics properties, such as wide optical bandgap, high electron mobility, high transparency in the visible and near infrared regions and suitable energy level match with perovskites, and simple fabrication of optically transparent dense films by several methods [98]. Miyasaka and colleagues have reported that PSCs with low-temperature processed SnO_2 as an ETLs exhibited a PCE of 13% with high stable [99]. Hagfeldt et al. have reported a simple chemical bath post-treatment deposited SnO_2 and used as ETL in PSCs that showed a PCE close to 21% [33]. In addition, You and co-workers have been achieved an impressive planar PSCs with a record PCE of 20.9% by incorporating of thin layer of SnO_2 nanoparticle as ETLs [100]. In order to further improve the performance of SnO_2 ETL based PSCs, the elemental doping and surface modification such as surface passivation and bilayer structure techniques have been employed. More importantly, elemental doping with various metal cations such as Li^+, and Sb^{3+} in SnO_2 ETLs exhibited efficient planar PSCs [101,102]. Furthermore, Fang and co-workers reported efficient PSCs with a PCE of 18% by using a 3-aminopropyltriethoxysilane self-assembled monolayer to modify the interface between the SnO_2 and perovskite [103]. The defect passivation technique has been used in SnO_2-based PSCs by using binary alkaline halides [104]. Yang et al. reported ethylene diaminetetraacetic acid (EDTA) modified SnO_2, where EDTA facilitates more smooth interface between SnO_2/perovskite and better match with the conduction band of perovskite, resulting in efficient

planar PSCs with a PCE of 21.52% [72]. Chen et al. reported PSCs with a PCE of 13.52% by inserting a simple spin-coating deposited SnO_2 onto TiO_2 CL owing to cover cracks of the TiO_2 hole-blocking layer [105]. Recently, Miyasaka and colleagues reported a stabilize high performance PSCs with a PCE of 22.1%, where TiO_2 CL was modified by the SnO_2 layer [70].

3.5. Zinc Oxide

ZnO is an outstanding inorganic semiconductor material because it is easy to synthesize, large surface area, and cost-effective fabrication. In addition, ZnO have been studied the most as CLs in PSCs because of their superior optoelectronic properties [106]. Recently, Kim and colleagues reported high-performance and stable PSCs by introducing SAM between ZnO ETL and perovskite in order to improve electron transfer from the perovskite layer to the ETL [32]. Cao et al. demonstrated an effective suppression of the corrosion of perovskite by incorporating the SnO_2 layer between ZnO and perovskite layers [75]. The PSCs exhibited PCEs as high as 12.17% with minimal hysteresis.

4. Other Metal Oxides

Other MO_x thin films such as WO_3 [36,107,108], Zn_2SnO_4 [109–112], Nb_2O_5 [37], In_2O_3 [113,114], $SrTiO_3$ [115,116], $BaTiO_3$ [117,118], $BaSnO_3$ [119,120], and ZrO_2 [35], have also been investigated for use as the potential CL in PSCs. The band gap of WO_3 is smaller compared to TiO_2, where it shows higher carrier mobility. Furthermore, Amassian and colleagues have demonstrated PSCs with a PCE of 11.24% by inserting a $TiCl_4$ layer at the perovskite/WO_3 interface, implying significantly reduced charge recombination [121]. Modifying the known ETLs by elemental doping and morphology treatment, along with discovering a new MO_x with superior properties, are required to further improve the performance and stability of PSCs.

5. Summary and Outlook

PSCs are attracting huge interest as next-generation thin-film photovoltaics with the hope of developing economically feasible power supplies to improve our environmental sustainability in the near future. However, several issues that currently hinder the commercialization of PSCs need to be considered, particularly their efficiency and stability. TiO_2 thin films have been widely used as ETLs in PSCs because of their excellent electrical properties, high durability, suitable energy-level match with perovskites, and easy fabrication of optically transparent dense films by several techniques. Recently, numerous attempts to improve device performance and stability through interface modification of TiO_2 CLs with different phases of TiO_2 NPs, elemental doping, and solvent engineering have been explored. Ideal ETL modification needs to be simple, conducted at low temperature, cost-effective, and provide an ETL with high thermal and chemical stability, suitable band alignment with the perovskite, and excellent wettability with perovskite precursor solution to yield efficient and stable PSCs suitable for future commercialization. From this perspective, we reviewed the progress of bilayer ETLs, which have improved both the performance and stability of PSCs.

To further improve the operational stability of PSCs, simultaneous device engineering such as interface modification of TiO_2 CL/perovskite, tuning of the crystallinity, morphology, and compositional engineering (both cations/halogens) of the perovskite along with optimization of the organic/inorganic HTL should be considered to realize their full potential. In addition, techniques suitable for large-area fabrication at low cost are highly desired to enable the development of large-area PSC modules. Further optimization of Pb-free perovskites may improve their sustainability to reach new heights in clean energy generation. Experiments should consider both the stability and efficiency of Pb-based and Pb-free PSCs to assist the solar energy revolution.

Author Contributions: Concept, M.S.; methodology, M.S.; visualization, M.A., J.-M.N. and T.T.; writing—original draft preparation, M.S.; review and editing, S.F., E.Y.M., L.W., M.N., M.A., M.K., K.T., J.-M.N. and T.T.; supervision, T.T. All authors have read and agreed to the published version of the manuscript.

Funding: This research received no external funding.

Acknowledgments: This research work was partially supported by a 2019 Research Grant from the Mitani Foundation for Research and Development.

Conflicts of Interest: The authors declare no conflict of interest.

References

1. Beggs, C. *Energy: Management, Supply and Conservation*; Elsevier Ltd.: Oxford, UK, 2012.
2. Priya, S.; Inman, D.J. *Energy Harvesting Technologies*; Springer Science: New York, NY, USA, 2008.
3. Green, M.A. Thin-film solar cells: Review of materials, technologies and commercial status. *J. Mater. Sci. Mater. Electron.* **2007**, *18*, 15–19. [CrossRef]
4. Sze, S.M.; Ng, K.K. *Physics of Semiconductor Devices*; John Wiley & Sons: Hoboken, NJ, USA, 2006.
5. Green, M.A. The path to 25% silicon solar cell efficiency: History of silicon cell evolution. *Prog. Photovolt. Res. Appl.* **2009**, *17*, 183–189. [CrossRef]
6. Park, N.-G. Perovskite solar cells: An emerging photovoltaic technology. *Mater. Today* **2015**, *18*, 65–72. [CrossRef]
7. Liu, Y.; Yang, Z.; Cui, D.; Ren, X.; Sun, J.; Liu, X.; Zhang, J.; Wei, Q.; Fan, H.; Yu, F.; et al. Two-inch-sized perovskite $CH_3NH_3PbX_3$ (X = Cl, Br, I) crystals: Growth and characterization. *Adv. Mater.* **2015**, *27*, 5176–5183. [CrossRef]
8. Luo, D.; Yang, W.; Wang, Z.; Sadhanala, A.; Hu, Q.; Su, R.; Shivanna, R.; Trindade, G.F.; Watts, J.F.; Xu, Z.; et al. Enhanced photovoltage for inverted planar heterojunction perovskite solar cells. *Science* **2018**, *360*, 1442–1446. [CrossRef]
9. Snaith, H.J. Perovskites: The emergence of a new era for low-cost, high-efficiency solar cells. *J. Phys. Chem. Lett.* **2013**, *4*, 3623–3630. [CrossRef]
10. Kojima, A.; Teshima, K.; Shirai, Y.; Miyasaka, T. Organometal halide perovskites as visible-light sensitizers for photovoltaic cells. *J. Am. Chem. Soc.* **2009**, *131*, 6050–6051. [CrossRef]
11. Best Research-Cell Efficiency Chart. Available online: https://www.nrel.gov/pv/assets/pdfs/pv-efficiencies-04-14-2020.pdf (accessed on 14 April 2020).
12. Yang, J.; Yuan, Z.; Liu, X.; Braun, S.; Li, Y.; Tang, J.; Gao, F.; Duan, C.-G.; Fahlman, M.; Bao, Q. Oxygen- and water-induced energetics degradation in organometal halide perovskites. *ACS Appl. Mater. Interfaces* **2018**, *10*, 16225–16230. [CrossRef]
13. Meng, L.; You, J.; Yang, Y. Addressing the stability issue of perovskite solar cells for commercial applications. *Nat. Commun.* **2018**, *9*, 5265. [CrossRef]
14. Wang, P.; Zhang, X.; Zhou, Y.; Jiang, Q.; Ye, Q.; Chu, Z.; Li, X.; Yang, X.; Yin, Z.; You, J. Solvent-controlled growth of inorganic perovskite films in dry environment for efficient and stable solar cells. *Nat. Commun.* **2018**, *9*, 2225. [CrossRef]
15. Arora, N.; Dar, M.I.; Hinderhofer, A.; Pellet, N.; Schreiber, F.; Zakeeruddin, S.M.; Grätzel, M. Perovskite solar cells with CuSCN hole extraction layers yield stabilized efficiencies greater than 20%. *Science* **2017**, *358*, 768–771. [CrossRef] [PubMed]
16. Jena, A.K.; Kulkarni, A.; Sanehira, Y.; Ikegami, M.; Miyasaka, T. Stabilization of α-$CsPbI_3$ in ambient room temperature conditions by incorporating Eu into $CsPbI_3$. *Chem. Mater.* **2018**, *30*, 6668–6674. [CrossRef]
17. Pant, N.; Kulkarni, A.; Yanagida, M.; Shirai, Y.; Miyasaka, T.; Miyano, K. Investigating the growth of $CH_3NH_3PbI_3$ Thin Films on RF-sputtered NiO_x for inverted planar perovskite solar cells: Effect of $CH_3NH_3^+$ halide additives versus $CH_3NH_3^+$ halide vapor annealing. *Adv. Mater. Interfaces* **2020**, *7*. [CrossRef]
18. Miyasaka, T.; Kulkarni, A.; Kim, G.M.; Öz, S.; Jena, A.K. Perovskite solar cells: Can we go organic-free, lead-free, and dopant-free? *Adv. Energy Mater.* **2020**, *10*, 1902500. [CrossRef]
19. Zong, Y.; Zhou, Y.; Zhang, Y.; Li, Z.; Zhang, L.; Ju, M.-G.; Chen, M.; Pang, S.; Zeng, X.C.; Padture, N.P. Continuous grain-boundary functionalization for high-efficiency perovskite solar cells with exceptional stability. *Chem* **2018**, *4*, 1404–1415. [CrossRef]
20. Saidaminov, M.I.; Kim, J.; Jain, A.; Quintero-Bermudez, R.; Tan, H.; Long, G.; Tan, F.; Johnston, A.; Zhao, Y.; Voznyy, O.; et al. Suppression of atomic vacancies via incorporation of isovalent small ions to increase the stability of halide perovskite solar cells in ambient air. *Nat. Energy* **2018**, *3*, 648–654. [CrossRef]

21. Chaudhary, B.; Kulkarni, A.; Jena, A.K.; Ikegami, M.; Udagawa, Y.; Kunugita, H.; Ema, K.; Miyasaka, T. Poly(4-vinylpyridine)-based interfacial passivation to enhance voltage and moisture stability of lead halide perovskite solar cells. *ChemSusChem* **2017**, *10*, 2473–2479. [CrossRef]
22. Yang, J.-M.; Luo, Y.; Bao, Q.; Li, Y.-Q.; Tang, J.-X. Hall of fame article: Recent advances in energetics and stability of metal halide perovskites for optoelectronic applications. *Adv. Mater. Interfaces* **2019**, *6*, 1801351. [CrossRef]
23. Burschka, J.; Pellet, N.; Moon, S.-J.; Humphry-Baker, R.; Gao, P.; Nazeeruddin, M.K.; Grätzel, M. Sequential deposition as a route to high-performance perovskite-sensitized solar cells. *Nature* **2013**, *499*, 316–319. [CrossRef]
24. Jeon, N.J.; Noh, J.H.; Kim, Y.C.; Yang, W.S.; Ryu, S.; Seok, S.I. Solvent engineering for high-performance inorganic–organic hybrid perovskite solar cells. *Nat. Mater.* **2014**, *13*, 897–903. [CrossRef]
25. Yang, W.S.; Noh, J.H.; Jeon, N.J.; Kim, Y.C.; Ryu, S.; Seo, J.; Seok, S.I. High-performance photovoltaic perovskite layers fabricated through intramolecular exchange. *Science* **2015**, *348*, 1234–1237. [CrossRef] [PubMed]
26. Bi, D.; Yi, C.; Luo, J.; Décoppet, J.-D.; Zhang, F.; Zakeeruddin, S.M.; Li, X.; Hagfeldt, A.; Grätzel, M. Polymer-templated nucleation and crystal growth of perovskite films for solar cells with efficiency greater than 21%. *Nat. Energy* **2016**, *1*, 16142. [CrossRef]
27. Yang, W.S.; Park, B.-W.; Jung, E.H.; Jeon, N.J.; Kim, Y.C.; Lee, D.U.; Shin, S.S.; Seo, J.; Kim, E.K.; Noh, J.H.; et al. Iodide management in formamidinium-lead-halide–based perovskite layers for efficient solar cells. *Science* **2017**, *356*, 1376–1379. [CrossRef] [PubMed]
28. Yu, X.; Marks, T.J.; Facchetti, A. Metal oxides for optoelectronic applications. *Nat. Mater.* **2016**, *15*, 383–396. [CrossRef]
29. Juarez-Perez, E.J.; Wuβler, M.; Fabregat-Santiago, F.; Lakus-Wollny, K.; Mankel, E.; Mayer, T.; Jaegermann, W.; Mora-Seró, I. Role of the selective contacts in the performance of lead halide perovskite solar cells. *J. Phys. Chem. Lett.* **2014**, *5*, 680–685. [CrossRef]
30. Moehl, T.; Im, J.H.; Lee, Y.H.; Domanski, K.; Giordano, F.; Zakeeruddin, S.M.; Dar, M.I.; Heiniger, L.-P.; Nazeeruddin, M.K.; Park, N.-G.; et al. Strong photocurrent amplification in perovskite solar cells with a porous TiO_2 blocking layer under reverse bias. *J. Phys. Chem. Lett.* **2014**, *5*, 3931–3936. [CrossRef] [PubMed]
31. Ke, W.; Fang, G.; Wang, J.; Qin, P.; Tao, H.; Lei, H.; Liu, Q.; Dai, X.; Zhao, X. Perovskite solar cell with an efficient TiO_2 compact film. *ACS Appl. Mater. Interfaces* **2014**, *6*, 15959–15965. [CrossRef]
32. Han, J.; Kwon, H.; Kim, E.; Kim, D.-W.; Son, H.J. Interfacial engineering of a ZnO electron transporting layer using self-assembled monolayers for high performance and stable perovskite solar cells. *J. Mater. Chem. A* **2020**, *8*, 2105–2113. [CrossRef]
33. Anaraki, E.H.; Kermanpur, A.; Steier, L.; Domanski, K.; Matsui, T.; Tress, W.R.; Saliba, M.; Abate, A.; Grätzel, M.; Hagfeldt, A.; et al. Highly efficient and stable planar perovskite solar cells by solution-processed tin oxide. *Energy Environ. Sci.* **2016**, *9*, 3128–3134. [CrossRef]
34. Azmi, R.; Hadmojo, W.T.; Sinaga, S.; Lee, C.-L.; Yoon, S.C.; Jung, I.H.; Jang, S.-Y. High-efficiency low-temperature ZnO based perovskite solar cells based on highly polar, nonwetting self-assembled molecular layers. *Adv. Energy Mater.* **2018**, *8*, 1701683. [CrossRef]
35. Mejía Escobar, M.A.; Pathak, S.; Liu, J.; Snaith, H.J.; Jaramillo, F. ZrO_2/TiO_2 Electron collection layer for efficient meso-superstructured hybrid perovskite solar cells. *ACS Appl. Mater. Interfaces* **2017**, *9*, 2342–2349. [CrossRef] [PubMed]
36. Gheno, A.; Pham, T.T.T.; Di Bin, C.; Bouclé, J.; Ratier, B.; Vedraine, S. Printable WO_3 electron transporting layer for perovskite solar cells: Influence on device performance and stability. *Sol. Energy Mater. Sol. Cells* **2017**, *161*, 347–354. [CrossRef]
37. Ling, X.; Yuan, J.; Liu, D.; Wang, Y.; Zhang, Y.; Chen, S.; Wu, H.; Jin, F.; Wu, F.; Shi, G.; et al. Room-temperature processed Nb_2O_5 as the electron-transporting layer for efficient planar perovskite solar cells. *ACS Appl. Mater. Interfaces* **2017**, *9*, 23181–23188. [CrossRef] [PubMed]
38. Hashimoto, K.; Irie, H.; Fujishima, A. TiO_2 Photocatalysis: A historical overview and future prospects. *Jpn. J. Appl. Phys.* **2005**, *44*, 8269–8285. [CrossRef]
39. O'Regan, B.; Grätzel, M.; Gr, M. A low-cost, high-efficiency solar cell based on dye-sensitized colloidal TiO_2 films. *Nature* **1991**, *353*, 737–740. [CrossRef]

40. Kim, H.-S.; Mora-Seró, I.; González-Pedro, V.; Fabregat-Santiago, F.; Juarez-Perez, E.J.; Park, N.-G.; Bisquert, J. Mechanism of carrier accumulation in perovskite thin-absorber solar cells. *Nat. Commun.* **2013**, *4*, 2242. [CrossRef]
41. Snaith, H.J.; Abate, A.; Ball, J.M.; Eperon, G.E.; Leijtens, T.; Noel, N.K.; Stranks, S.D.; Wang, J.T.-W.; Wojciechowski, K.; Zhang, W. Anomalous hysteresis in perovskite solar cells. *J. Phys. Chem. Lett.* **2014**, *5*, 1511–1515. [CrossRef]
42. Leijtens, T.; Eperon, G.E.; Pathak, S.; Abate, A.; Lee, M.M.; Snaith, H.J. Overcoming ultraviolet light instability of sensitized TiO_2 with meso-superstructured organometal tri-halide perovskite solar cells. *Nat. Commun.* **2013**, *4*, 2885. [CrossRef]
43. Ito, S.; Tanaka, S.; Manabe, K.; Nishino, H. Effects of surface blocking layer of Sb_2S_3 on nanocrystalline TiO_2 for $CH_3NH_3PbI_3$ perovskite solar cells. *J. Phys. Chem. C* **2014**, *118*, 16995–17000. [CrossRef]
44. Singh, T.; Öz, S.; Sasinska, A.; Frohnhoven, R.; Mathur, S.; Miyasaka, T. Sulfate-assisted interfacial engineering for high yield and efficiency of triple cation perovskite solar cells with alkali-doped TiO_2 electron-transporting layers. *Adv. Funct. Mater.* **2018**, *28*, 1706287. [CrossRef]
45. Mohammadian-Sarcheshmeh, H.; Mazloum-Ardakani, M. Recent advancements in compact layer development for perovskite solar cells. *Heliyon* **2018**, *4*, e00912. [CrossRef] [PubMed]
46. Liu, M.; Johnston, M.B.; Snaith, H.J. Efficient planar heterojunction perovskite solar cells by vapour deposition. *Nature* **2013**, *501*, 395–398. [CrossRef] [PubMed]
47. Shahiduzzaman, M.; Yamamoto, K.; Furumoto, Y.; Kuwabara, T.; Takahashi, K.; Taima, T. Enhanced photovoltaic performance of perovskite solar cells via modification of surface characteristics using a fullerene interlayer. *Chem. Lett.* **2015**, *44*, 1735–1737. [CrossRef]
48. Shahiduzzaman, M.; Karakawa, M.; Yamamoto, K.; Kusumi, T.; Yonezawa, K.; Kuwabara, T.; Takahashi, K.; Taima, T. Interface engineering of compact-TiO_x in planar perovskite solar cells using low-temperature processable high-mobility fullerene derivative. *Sol. Energy Mater. Sol. Cells* **2018**, *178*, 1–7. [CrossRef]
49. Noh, J.H.; Im, S.H.; Heo, J.H.; Mandal, T.N.; Seok, S.I. Chemical management for colorful, efficient, and stable inorganic–organic hybrid nanostructured solar cells. *Nano Lett.* **2013**, *13*, 1764–1769. [CrossRef] [PubMed]
50. Wu, Y.; Yang, X.; Chen, H.; Zhang, K.; Qin, C.; Liu, J.; Peng, W.; Islam, A.; Bi, E.; Ye, F.; et al. Highly compact TiO_2 layer for efficient hole-blocking in perovskite solar cells. *Appl. Phys. Express* **2014**, *7*, 052301. [CrossRef]
51. Chen, C.; Cheng, Y.; Dai, Q.; Song, H. Radio frequency magnetron sputtering deposition of TiO_2 thin films and their perovskite solar cell applications. *Sci. Rep.* **2015**, *5*, 17684. [CrossRef]
52. Maruyama, T.; Arai, S. Titanium dioxide thin films prepared by chemical vapor deposition. *Sol. Energy Mater. Sol. Cells* **1992**, *26*, 323–329. [CrossRef]
53. Su, T.-S.; Hsieh, T.-Y.; Hong, C.-Y.; Wei, T.-C. Electrodeposited ultrathin TiO_2 blocking layers for efficient perovskite solar cells. *Sci. Rep.* **2015**, *5*, 16098. [CrossRef]
54. Cojocaru, L.; Uchida, S.; Sanehira, Y.; Nakazaki, J.; Kubo, T.; Segawa, H. Surface treatment of the compact TiO_2 layer for efficient planar heterojunction perovskite solar cells. *Chem. Lett.* **2015**, *44*, 674–676. [CrossRef]
55. Zhou, H.; Chen, Q.; Li, G.; Luo, S.; Song, T.-B.; Duan, H.-S.; Hong, Z.; You, J.; Liu, Y.; Yang, Y. Interface engineering of highly efficient perovskite solar cells. *Science* **2014**, *345*, 542–546. [CrossRef]
56. Deng, X.; Wilkes, G.C.; Chen, A.Z.; Prasad, N.S.; Gupta, M.C.; Choi, J.J. Room-temperature processing of TiO_x electron transporting layer for perovskite solar cells. *J. Phys. Chem. Lett.* **2017**, *8*, 3206–3210. [CrossRef] [PubMed]
57. Liu, Z.; Chen, Q.; Hong, Z.; Zhou, H.; Xu, X.; De Marco, N.; Sun, P.; Zhao, Z.; Cheng, Y.-B.; Yang, Y. Low-temperature TiO_x compact layer for planar heterojunction perovskite solar cells. *ACS Appl. Mater. Interfaces* **2016**, *8*, 11076–11083. [CrossRef] [PubMed]
58. Shahiduzzaman, M.; Yonezawa, K.; Yamamoto, K.; Ripolles, T.S.; Karakawa, M.; Kuwabara, T.; Takahashi, K.; Hayase, S.; Taima, T. Improved reproducibility and intercalation control of efficient planar inorganic perovskite solar cells by simple alternate vacuum deposition of PbI_2 and CsI. *ACS Omega* **2017**, *2*, 4464–4469. [CrossRef] [PubMed]
59. Ren, X.; Xie, L.; Kim, W.B.; Lee, D.G.; Jung, H.S.; Liu, S. Chemical bath deposition of co-doped TiO_2 electron transport layer for hysteresis-suppressed high-efficiency planar perovskite solar cells. *Sol. RRL* **2019**, *3*, 1900176. [CrossRef]

60. Kuwabara, T.; Sugiyama, H.; Kuzuba, M.; Yamaguchi, T.; Takahashi, K. Inverted bulk-heterojunction organic solar cell using chemical bath deposited titanium oxide as electron collection layer. *Org. Electron.* **2010**, *11*, 1136–1140. [CrossRef]
61. Adhikari, T.; Shahiduzzaman, M.; Yamamoto, K.; Lebel, O.; Nunzi, J.-M. Interfacial modification of the electron collecting layer of low-temperature solution-processed organometallic halide photovoltaic cells using an amorphous perylenediimide. *Sol. Energy Mater. Sol. Cells* **2017**, *160*, 294–300. [CrossRef]
62. Shahiduzzaman, M.; Yamamoto, K.; Furumoto, Y.; Kuwabara, T.; Takahashi, K.; Taima, T. Ionic liquid-assisted growth of methylammonium lead iodide spherical nanoparticles by a simple spin-coating method and photovoltaic properties of perovskite solar cells. *RSC Adv.* **2015**, *5*, 77495–77500. [CrossRef]
63. Taima, T.; Shahiduzzaman, M.; Yamamoto, K.; Furumoto, Y.; Kuwabara, T.; Takahashi, K. Planar heterojunction type perovskite solar cells based on TiO_x compact layer fabricated by chemical bath deposition. In *Oxide-based Materials and Devices VII*; International Society for Optics and Photonics: Bellingham, WA, USA, 2016; Volume 9749, p. 97491G. [CrossRef]
64. Shahiduzzaman, M.; Sakuma, T.; Kaneko, T.; Tomita, K.; Isomura, M.; Taima, T.; Umezu, S.; Iwamori, S. Oblique electrostatic inkjet-deposited TiO_2 electron transport layers for efficient planar perovskite solar cells. *Sci. Rep.* **2019**, *9*, 1–8. [CrossRef]
65. Shahiduzzaman, M.; Ashikawa, H.; Kuniyoshi, M.; Visal, S.; Sakakibara, S.; Kaneko, T.; Katsumata, T.; Taima, T.; Iwamori, S.; Isomura, M.; et al. Compact TiO_2/Anatase TiO_2 single-crystalline nanoparticle electron-transport bilayer for efficient planar perovskite solar cells. *ACS Sustain. Chem. Eng.* **2018**, *6*, 12070–12078. [CrossRef]
66. Shahiduzzaman, M.; Visal, S.; Kuniyoshi, M.; Kaneko, T.; Umezu, S.; Katsumata, T.; Iwamori, S.; Kakihana, M.; Taima, T.; Isomura, M.; et al. Low-temperature-processed brookite-based TiO_2 heterophase junction enhances performance of planar perovskite solar cells. *Nano Lett.* **2018**, *19*, 598–604. [CrossRef] [PubMed]
67. Shahiduzzaman, M.; Kulkarni, A.; Visal, S.; Wang, L.; Nakano, M.; Karakawa, M.; Takahashi, K.; Umezu, S.; Masuda, A.; Iwamori, S.; et al. A single-phase brookite TiO_2 nanoparticle bridge enhances the stability of perovskite solar cells. *Sustain. Energy Fuels* **2020**, *4*, 2009–2017. [CrossRef]
68. Li, X.; Dai, S.-M.; Zhu, P.; Deng, L.-L.; Xie, S.-Y.; Cui, Q.; Chen, H.; Wang, N.; Lin, H. Efficient perovskite solar cells depending on TiO_2 Nanorod Arrays. *ACS Appl. Mater. Interfaces* **2016**, *8*, 21358–21365. [CrossRef]
69. Lee, Y.; Paek, S.; Cho, K.T.; Oveisi, E.; Gao, P.; Lee, S.; Park, J.-S.; Zhang, Y.; Humphry-Baker, R.; Asiri, A.M.; et al. Enhanced charge collection with passivation of the tin oxide layer in planar perovskite solar cells. *J. Mater. Chem. A* **2017**, *5*, 12729–12734. [CrossRef]
70. Kim, G.M.; Ishii, A.; Öz, S.; Miyasaka, T. MACl-assisted Ge doping of Pb-hybrid perovskite: A universal route to stabilize high performance perovskite solar cells. *Adv. Energy Mater.* **2020**, *10*, 1903299. [CrossRef]
71. Song, S.; Kang, G.; Pyeon, L.; Lim, C.; Lee, G.-Y.; Park, T.; Choi, J. Systematically optimized bilayered electron transport layer for highly efficient planar perovskite solar cells (η = 21.1%). *ACS Energy Lett.* **2017**, *2*, 2667–2673. [CrossRef]
72. Yang, D.; Yang, R.; Wang, K.; Wu, C.; Zhu, X.; Feng, J.; Ren, X.; Fang, G.; Priya, S.; Liu, S. High efficiency planar-type perovskite solar cells with negligible hysteresis using EDTA-complexed SnO_2. *Nat. Commun.* **2018**, *9*, 3239. [CrossRef]
73. Zuo, L.; Chen, Q.; De Marco, N.; Hsieh, Y.-T.; Chen, H.; Sun, P.; Chang, S.-Y.; Zhao, H.; Dong, S.; Yang, Y. Tailoring the Interfacial Chemical Interaction for High-Efficiency Perovskite Solar Cells. *Nano Lett.* **2016**, *17*, 269–275. [CrossRef]
74. Ke, W.; Zhao, D.; Xiao, C.; Wang, C.; Cimaroli, A.J.; Grice, C.; Yang, M.; Li, Z.; Jiang, C.-S.; Al-Jassim, M.; et al. Cooperative tin oxide fullerene electron selective layers for high-performance planar perovskite solar cells. *J. Mater. Chem. A* **2016**, *4*, 14276–14283. [CrossRef]
75. Wang, P.; Zhao, J.; Liu, J.; Wei, L.; Liu, Z.; Guan, L.; Cao, G. Stabilization of organometal halide perovskite films by SnO_2 coating with inactive surface hydroxyl groups on ZnO nanorods. *J. Power Sources* **2017**, *339*, 51–60. [CrossRef]
76. Tomita, K.; Kobayashi, M.; Petrykin, V.; Yin, S.; Sato, T.; Yoshimura, M.; Kakihana, M. Hydrothermal synthesis of TiO_2 nano-particles using novel water-soluble titanium complexes. *J. Mater. Sci.* **2007**, *43*, 2217–2221. [CrossRef]
77. Gan, X.; Wang, O.; Liu, K.; Du, X.; Guo, L.; Liu, H. 2D homologous organic-inorganic hybrids as light-absorbers for planer and nanorod-based perovskite solar cells. *Sol. Energy Mater. Sol. Cells* **2017**, *162*, 93–102. [CrossRef]

78. He, X.; Wu, J.; Tu, Y.; Xie, Y.; Dong, J.; Jia, J.; Wei, Y.; Lan, Z. TiO_2 single crystalline nanorod compact layer for high-performance $CH_3NH_3PbI_3$ perovskite solar cells with an efficiency exceeding 17%. *J. Power Sources* **2016**, *332*, 366–371. [CrossRef]
79. Wei, D.; Ji, J.; Song, D.; Li, M.; Cui, P.; Li, Y.; Mbengue, J.M.; Zhou, W.; Ning, Z.; Park, N.-G. A TiO_2 embedded structure for perovskite solar cells with anomalous grain growth and effective electron extraction. *J. Mater. Chem. A* **2017**, *5*, 1406–1414. [CrossRef]
80. Choi, M.; Lim, J.; Baek, M.; Choi, W.; Kim, W.; Yong, K. Investigating the unrevealed photocatalytic activity and stability of nanostructured brookite TiO_2 film as an environmental photocatalyst. *ACS Appl. Mater. Interfaces* **2017**, *9*, 16252–16260. [CrossRef]
81. Zhao, M.; Li, L.; Lin, H.; Yang, L.; Li, G. A facile strategy to fabricate large-scale uniform brookite TiO_2 nanospindles with high thermal stability and superior electrical properties. *Chem. Commun.* **2013**, *49*, 7046. [CrossRef]
82. Mo, S.-D.; Ching, W.Y. Electronic and optical properties of three phases of titanium dioxide: Rutile, anatase, and brookite. *Phys. Rev. B* **1995**, *51*, 13023–13032. [CrossRef]
83. Kogo, A.; Sanehira, Y.; Numata, Y.; Ikegami, M.; Miyasaka, T. Amorphous metal oxide blocking layers for highly efficient low-temperature brookite TiO_2-based perovskite solar cells. *ACS Appl. Mater. Interfaces* **2018**, *10*, 2224–2229. [CrossRef]
84. Qiu, J.; Qiu, Y.; Yan, K.; Zhong, M.; Mu, C.; Yan, H.; Yang, S. All-solid-state hybrid solar cells based on a new organometal halide perovskite sensitizer and one-dimensional TiO_2 nanowire arrays. *Nanoscale* **2013**, *5*, 3245–3248. [CrossRef]
85. Yang, M.; Guo, R.; Kadel, K.; Liu, Y.; O'Shea, K.; Bone, R.; Wang, X.; He, J.; Li, W. Improved charge transport of Nb-doped TiO_2 nanorods in methylammonium lead iodide bromide perovskite solar cells. *J. Mater. Chem. A* **2014**, *2*, 19616–19622. [CrossRef]
86. Zhang, X.; Bao, Z.; Tao, X.; Sun, H.; Chen, W.; Zhou, X. Sn-doped TiO_2 nanorod arrays and application in perovskite solar cells. *RSC Adv.* **2014**, *4*, 64001–64005. [CrossRef]
87. Kim, H.-S.; Lee, J.-W.; Yantara, N.; Boix, P.P.; Kulkarni, S.A.; Mhaisalkar, S.; Grätzel, M.; Park, N.-G. High Efficiency Solid-State Sensitized Solar Cell-Based on Submicrometer Rutile TiO_2 nanorod and $CH_3NH_3PbI_3$ Perovskite Sensitizer. *Nano Lett.* **2013**, *13*, 2412–2417. [CrossRef] [PubMed]
88. Lee, J.-W.; Lee, T.-Y.; Yoo, P.J.; Grätzel, M.; Mhaisalkar, S.; Park, N.-G. Rutile TiO_2-based perovskite solar cells. *J. Mater. Chem. A* **2014**, *2*, 9251. [CrossRef]
89. Wu, S.; Cheng, C.; Jin, J.; Wang, J.; Peng, T. Low-temperature processed nanostructured rutile TiO_2 array films for perovskite solar cells with high efficiency and stability. *Sol. RRL* **2017**, *2*, 1700164. [CrossRef]
90. Liang, C.; Wu, Z.; Li, P.; Fan, J.; Zhang, Y.; Shao, G. Chemical bath deposited rutile TiO_2 compact layer toward efficient planar heterojunction perovskite solar cells. *Appl. Surf. Sci.* **2017**, *391*, 337–344. [CrossRef]
91. Giordano, F.; Abate, A.; Correa-Baena, J.-P.; Saliba, M.; Matsui, T.; Im, S.H.; Zakeeruddin, S.M.; Nazeeruddin, M.K.; Hagfeldt, A.; Graetzel, M. Enhanced electronic properties in mesoporous TiO_2 via lithium doping for high-efficiency perovskite solar cells. *Nat. Commun.* **2016**, *7*, 10379. [CrossRef]
92. Huckaba, A.J.; Lee, Y.; Xia, R.; Paek, S.; Bassetto, V.C.; Oveisi, E.; Lesch, A.; Kinge, S.; Dyson, P.J.; Girault, H.; et al. Inkjet-printed mesoporous TiO_2 and perovskite layers for high efficiency perovskite solar cells. *Energy Technol.* **2019**, *7*, 186. [CrossRef]
93. Sung, S.D.; Ojha, D.P.; You, J.S.; Lee, J.; Kim, J.; Lee, W.I. 50 nm sized spherical TiO_2 nanocrystals for highly efficient mesoscopic perovskite solar cells. *Nanoscale* **2015**, *7*, 8898–8906. [CrossRef]
94. Wang, J.T.-W.; Ball, J.M.; Barea, E.; Abate, A.; Alexander-Webber, J.; Huang, J.; Saliba, M.; Mora-Seró, I.; Bisquert, J.; Snaith, H.J.; et al. Low-temperature processed electron collection layers of graphene/TiO_2 nanocomposites in thin film perovskite solar cells. *Nano Lett.* **2013**, *14*, 724–730. [CrossRef]
95. Huang, A.; Lei, L.; Zhu, J.; Yu, Y.; Liu, Y.; Yang, S.; Bao, S.; Jin, P. Controllable deposition of TiO_2 nanopillars at room temperature for high performance perovskite solar cells with suppressed hysteresis. *Sol. Energy Mater. Sol. Cells* **2017**, *168*, 172–182. [CrossRef]
96. Shin, S.S.; Lee, S.J.; Seok, S.I. Metal oxide charge transport layers for efficient and stable perovskite solar cells. *Adv. Funct. Mater.* **2019**, *29*, 1900455. [CrossRef]
97. Singh, T.; Miyasaka, T.; Singh, J. ChemInform abstract: Role of metal oxide electron-transport layer modification on the stability of high performing perovskite solar cells. *ChemSusChem* **2016**, *47*, 2559–2566. [CrossRef] [PubMed]

98. Xiong, L.; Guo, Y.; Wen, J.; Liu, H.; Yang, G.; Qin, P.; Fang, G. Review on the application of SnO_2 in perovskite solar cells. *Adv. Funct. Mater.* **2018**, *28*, 1802757. [CrossRef]
99. Song, J.; Zheng, E.; Bian, J.; Wang, X.-F.; Tian, W.; Sanehira, Y.; Miyasaka, T. Low-temperature SnO_2-based electron selective contact for efficient and stable perovskite solar cells. *J. Mater. Chem. A* **2015**, *3*, 10837–10844. [CrossRef]
100. Jiang, Q.; Chu, Z.; Wang, P.; Yang, X.; Liu, H.; Wang, Y.; Yin, Z.; Wu, J.; Zhang, Y.; You, J. Planar-structure perovskite solar cells with efficiency beyond 21%. *Adv. Mater.* **2017**, *29*, 1703852. [CrossRef]
101. Bai, Y.; Fang, Y.; Deng, Y.; Wang, Q.; Zhao, J.; Zheng, X.; Zhang, Y.; Huang, J. Low-temperature solution-processed Sb:SnO_2 nanocrystals for efficient planar perovskite solar cells. *ChemSusChem* **2016**, *9*, 2686–2691. [CrossRef]
102. Park, M.; Kim, J.-Y.; Son, H.J.; Lee, C.-H.; Jang, S.S.; Ko, M.J. Low-temperature solution-processed Li-doped SnO_2 as an effective electron transporting layer for high-performance flexible and wearable perovskite solar cells. *Nano Energy* **2016**, *26*, 208–215. [CrossRef]
103. Yang, G.; Wang, C.; Lei, H.; Zheng, X.; Qin, P.; Xiong, L.; Zhao, X.; Yan, Y.; Fang, G. Interface engineering in planar perovskite solar cells: Energy level alignment, perovskite morphology control and high performance achievement. *J. Mater. Chem. A* **2017**, *5*, 1658–1666. [CrossRef]
104. Wang, P.; Wang, J.; Zhang, X.; Wang, H.; Cui, X.; Yuan, S.; Lu, H.; Tu, L.; Zhan, Y.; Zheng, L. Boosting the performance of perovskite solar cells through a novel active passivation method. *J. Mater. Chem. A* **2018**, *6*, 15853–15858. [CrossRef]
105. Ren, H.; Zou, X.; Cheng, J.; Ling, T.; Bai, X.; Chen, D. Facile solution spin-coating SnO_2 thin film covering cracks of TiO_2 hole blocking layer for perovskite solar cells. *Coatings* **2018**, *8*, 314. [CrossRef]
106. Zhang, D.; Zhang, X.; Bai, S.; Liu, C.; Li, Z.; Guo, W.; Gao, F. Surface chlorination of ZnO for perovskite solar cells with enhanced efficiency and stability. *Sol. RRL* **2019**, *3*, 1900154. [CrossRef]
107. Ali, F.; Pham, N.D.; Fan, L.; Tiong, V.; Dai, X.; Bell, J.M.; Wang, H.; Tesfamichael, T.; Ostrikov, K. Low hysteresis perovskite solar cells using an electron-beam evaporated WO_{3-x} thin film as the electron transport layer. *ACS Appl. Energy Mater.* **2019**, *2*, 5456–5464. [CrossRef]
108. You, Y.; Tian, W.; Min, L.; Cao, F.; Deng, K.; Li, L. TiO_2/WO_3 bilayer as electron transport layer for efficient planar perovskite solar cell with efficiency exceeding 20%. *Adv. Mater. Interfaces* **2020**, *7*, 1901406. [CrossRef]
109. Dou, J.; Zhang, Y.; Wang, Q.; Abate, A.; Li, Y.; Wei, M. Highly efficient Zn_2SnO_4 perovskite solar cells through band alignment engineering. *Chem. Commun.* **2019**, *55*, 14673–14676. [CrossRef] [PubMed]
110. Dou, J.; Shen, D.; Li, Y.; Abate, A.; Wei, M. Highly efficient perovskite solar cells based on a Zn_2SnO_4 compact layer. *ACS Appl. Mater. Interfaces* **2019**, *11*, 36553–36559. [CrossRef] [PubMed]
111. Zheng, M.; Xu, W.; Yuan, H.; Wu, J. Mesostructured perovskite solar cells based on Zn_2SnO_4 single crystal mesoporous layer with efficiency of 18.32%. *J. Alloys Compd.* **2020**, *823*, 153730. [CrossRef]
112. Shin, S.S.; Yang, W.S.; Noh, J.H.; Suk, J.H.; Jeon, N.J.; Park, J.H.; Kim, J.S.; Seong, W.M.; Seok, S.I. High-performance flexible perovskite solar cells exploiting Zn_2SnO_4 prepared in solution below 100 °C. *Nat. Commun.* **2015**, *6*, 7410. [CrossRef]
113. Chen, P.; Yin, X.; Que, M.; Yang, Y.; Liu, X.; Que, W. Bilayer photoanode approach for efficient In_2O_3 based planar heterojunction perovskite solar cells. *J. Alloy. Compd.* **2018**, *735*, 938–944. [CrossRef]
114. Yoon, S.; Kim, S.J.; Kim, H.S.; Park, J.-S.; Han, I.K.; Jung, J.W.; Park, M. Solution-processed indium oxide electron transporting layers for high-performance and photo-stable perovskite and organic solar cells. *Nanoscale* **2017**, *9*, 16305–16312. [CrossRef]
115. Okamoto, Y.; Fukui, R.; Fukazawa, M.; Suzuki, Y. $SrTiO_3$/TiO_2 composite electron transport layer for perovskite solar cells. *Mater. Lett.* **2017**, *187*, 111–113. [CrossRef]
116. Mahmoudi, T.; Wang, Y.; Hahn, Y.-B. $SrTiO_3$/Al_2O_3-graphene electron transport layer for highly stable and efficient composites-based perovskite solar cells with 20.6% efficiency. *Adv. Energy Mater.* **2020**, *10*, 1903369. [CrossRef]
117. Qin, J.; Zhang, Z.; Shi, W.; Liu, Y.; Gao, H.; Mao, Y. Enhanced performance of perovskite solar cells by using ultrathin $BaTiO_3$ interface modification. *ACS Appl. Mater. Interfaces* **2018**, *10*, 36067–36074. [CrossRef] [PubMed]
118. Okamoto, Y.; Suzuki, Y. Mesoporous $BaTiO_3$/TiO_2 double layer for electron transport in perovskite solar cells. *J. Phys. Chem. C* **2016**, *120*, 13995–14000. [CrossRef]

119. Shin, S.S.; Yeom, E.J.; Yang, W.S.; Hur, S.; Kim, M.G.; Im, J.; Seo, J.; Noh, J.H.; Seok, S.I. Colloidally prepared La-doped $BaSnO_3$ electrodes for efficient, photostable perovskite solar cells. *Science* **2017**, *356*, 167–171. [CrossRef] [PubMed]
120. Zhu, L.; Ye, J.; Zhang, X.; Zheng, H.; Liu, G.; Pan, X.; Dai, S. Performance enhancement of perovskite solar cells using a La-doped $BaSnO_3$ electron transport layer. *J. Mater. Chem. A* **2017**, *5*, 3675–3682. [CrossRef]
121. Mahmood, K.; Swain, B.S.; Kirmani, A.R.; Amassian, A. Highly efficient perovskite solar cells based on a nanostructured WO_3–TiO_2 core–shell electron transporting material. *J. Mater. Chem. A* **2015**, *3*, 9051–9057. [CrossRef]